Miniband electronic structure of quantum dash array

B. M. Stupovski, J. V. Crnjanski, and D. M. Gvozdić
Faculty of Electrical Engineering, University of Belgrade, Bulevar Kralja Aleksandra 73b, P.O. Box 35-54, 11120 Belgrade, Serbia

(Received 17 October 2012; accepted 19 November 2012; published online 21 December 2012)

In the paper, we investigate the miniband structure of one-dimensional quantum dash array and its dependence on geometrical parameters by using a newly developed and efficient numerical method. We show that miniband energy significantly depends on the dash height and width, while the miniband width depends on the array period and the dash width. The excited minibands may exhibit the effect of zero miniband gap and the multiple anticrossings, which are followed by the swapping of the character of adjacent minibands top and bottom. The wetting layer allows formation of a miniband cluster in the vicinity of the well top, which essentially represents the barrier continuum embedded into the well of array. © *2012 American Institute of Physics*. [http://dx.doi.org/10.1063/1.4770437]

I. INTRODUCTION

Recent studies have shown that photonic devices incorporating semiconductor nanostructures in which the electronic motion is confined in more than one spatial direction, may overcome some of the limitations of quantum well based devices, especially short excited-state carrier lifetime,[1] caused by numerous in-plane scattering paths.[2] Self-assembled nanostructures, as three-dimensionally (3D) confined quantum dots (QDs) or their elongated version with 2D confinement, called quantum dashes (QDH), may provide the additional confinement required for reduction of scattering events or improvement of optical transitions strength and polarization. Therefore, investigation of their electronic structure is a basis for further understanding and optimization with respect to carrier scattering processes and its lifetime, optical transitions strength and polarization type.

The electronic band structure in these nanostructures is usually studied thoroughly for an isolated system comprising the well and the barrier region and corresponding strain and potential distribution.[3–8] However, due to self-assembled growth, these nanostructures form an ensemble in which dots or dashes are usually distributed in the close proximity of each other, leading to a quantum mechanical coupling.[9] Due to the coupling, the electronic band structure as well as the optical properties of these nanostructures may significantly differ from those for an isolated dot or dash.

In this paper, we present an efficient numerical method, based on coordinate transformation and the finite differences method, which provides calculation of electronic band structure of quantum dash array. In the case of sufficiently high compressive strain, which is common for QDHs, it is possible to consider heavy and light holes decoupled and apply this method even in the calculation of the QDH valence band structure.[5,9] Due to a stochastic distribution, QDH array may consist of dashes with different cross-section, which means that their width, height, shape and even separation of adjacent dashes might be different.[8–11] However, our model is based on the assumption that the QDH ensemble consists of equally long dashes with the same cross-section profile distributed in a periodic array. Although the model can not provide precise insight into electronic band structure of array consisting of QDHs with randomized cross-section dimensions, it can help to understand and reveal the influence of different geometrical parameters of the QDH array on the electronic band structure. Therefore, we investigate how the QDH width and height as well as the period of array, affect electronic states in the QDH conduction band.

We focus our investigation on two different material systems. As first, we study InAs/InAlGaAs QDHs, where InAlGaAs is latticed matched to InP. Although this material system is useful for telecom applications due to interband emission at 1.5 μm, it was recently implemented as the active region of a quantum cascade laser.[2] However, the well in this material system is shallow and doesn't provide sufficient depth for different minibands and effects which may occur in deeper wells. Thus, we extend our research on InAs/GaAs QDHs, which due to a larger depth exhibit more interesting effects in the electronic band structure.

In Sec. II, we give details of our method, which combines specially designed coordinate mappings and finite differences for calculation of electronic band structure. In Sec. III, we present application of the method to InAs/InAlGaAs QDH array. In this section, we show and discuss how electronic minibands depend on the QDH height, full width at half of the height, and the array period, and compare results obtained for different material systems. In the last section we present conclusions of this paper.

II. DESCRIPTION OF THE METHOD

In our analysis of minibands, we take into account the wetting layer (WL), formed as a consequence of self-assembled growth of InAs islands. The strength of quantum mechanical coupling between dashes in the QDH material depends on the WL thickness (t_W) and the density of QDHs, as well as on the actual profile of the QDH's cross-section. The WL thickness t_W is defined as the well material thickness in the middle of two neighbouring QDHs [Fig. 1(a)]. Parameters of the QDH cross section are the maximum

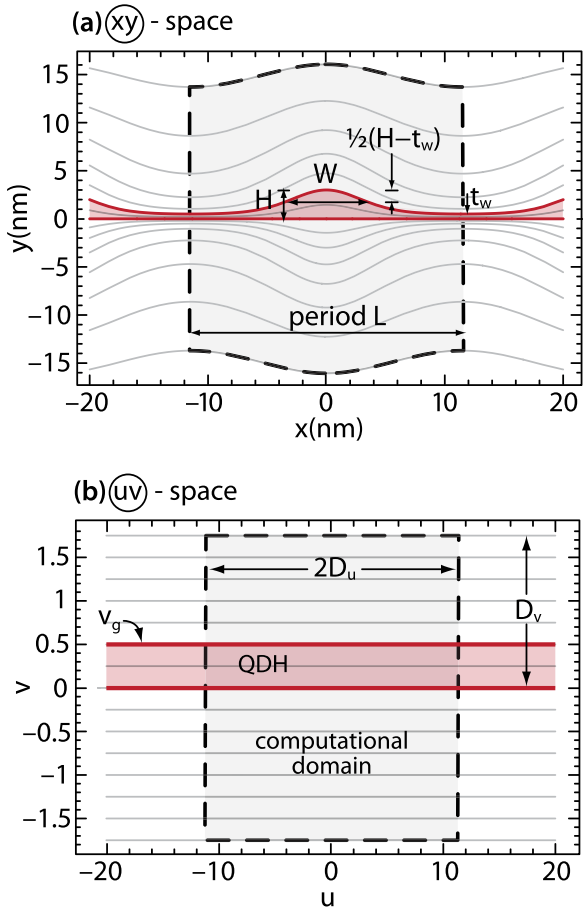

FIG. 1. The cross-section profile of QDH array and the computational domain in (a) the real *xy*-space, and in (b) the mapped *uv*-space. Dashed lines represent boundaries of the computational domain and the elementary cell of the QDH array.

height of the QDH array denoted by H, and the full width at half maximum W of a single QDH with respect to the wetting layer thickness [Fig. 1(a)]. Material parameters and the conduction band offset (Table I) are taken from Refs. 12 and 13, assuming compressively strained dashes.[9] Since QDHs exhibit the quantum-wire like nature,[4] we approximate them with infinitely long wires and focus only on their profile of carrier confinement in the transversal x-y plane [Fig. 1(a)]. Thus, the quantization in the longitudinal z-direction leads to a quasi-continuous subband structure, the energy of which is well approximated with parabolic dependence on corresponding wave vector k_z.

The conduction band structure of the periodic array of QDHs is modelled by using the single-band Schrödinger equation in the envelope function approximation:

$$-\frac{\hbar^2}{2}\left[\frac{\partial}{\partial x}\left(\frac{1}{m^*}\frac{\partial\psi}{\partial x}\right)+\frac{\partial}{\partial y}\left(\frac{1}{m^*}\frac{\partial\psi}{\partial y}\right)\right]+\left[\frac{\hbar^2 k_z^2}{2m^*}+U\right]\psi=E\psi, \tag{1}$$

TABLE I. Material parameters used for band calculation.

	InAs	GaAs	$In_{0.53}Ga_{0.23}Al_{0.24}As$
$m^*(m_0)$	0.0221	0.0623	0.0547
ΔE_c(meV)		858.7	396.9

where $\psi=\psi(x,y)$ is slowly varying part of the total wavefunction, $U=U(x,\ y)$ is the 2D potential profile determined by the heterointerface of the well and the matrix material and the conduction band offset ΔE_c, $m^*=m^*(x,y)$ is the electronic effective mass, while E is the confinement energy referenced to the conduction band edge of the QDH barrier material. In our analysis, we are interested only in the eigenenergies corresponding to the subband bottom, for which $k_z=0$.

Although realistic QDH ensemble comprises nonuniformly distributed InAs islands, in our calculation we analyze the array of identical QDHs equally spaced in the x-direction. Therefore solution of Eq. (1) satisfies Bloch theorem for the wave function $\psi(x,y)$ in periodic potential:

$$\psi(x+L,y)=\exp(\imath KL)\psi(x,y), \tag{2}$$

where L is the period of QDH array in the x-direction, while K is Bloch wave number (miniband wavevector). The extreme values of the phase shift factor $\exp(\imath KL)$, $+1$ and -1, corresponding to $KL=0$ and $KL=\pi$, respectively, determine boundaries of the minibands and corresponding wavefunctions. Since the periodicity exists only in the x-direction, while in the y-direction there is no coupling between dashes, formation of the minibands is limited to the range of energies below the band edge of the QDH barrier material. The full periodicity can be achieved by stacking additional arrays of quantum dashes on the top of each other. In this case, the minibands can be formed in and above the well. In the paper, we focus on the single array of QDHs.

Depending on the material system, nominal thickness of the InAs layer and growth parameters, e.g. the growth temperature, group-III/V ratio and growth rate, self-assembled QDHs may have different dimensions and shapes of the cross-section profiles.[8–11] Thus, the functions used for coordinate transformation and the QDH cross-section profile fitting may differ significantly. Before we proceed with a detailed description of these functions, we generally present the method used for calculation of the electronic band structure.

The method is based on the combination of coordinate transformation and the finite differences method (FDM).[12] Essentially, the coordinate transformation maps the well, i.e., the profile of the dash array cross-section, and surrounding barrier space, which has to be sufficiently large to naturally accommodate the wavefunctions [Fig. 1(a)], into the computational domain with straight boundaries and heterointerfaces [Fig. 1(b)]. Since we apply the periodic boundary condition (2), the computational domain in the x-direction is limited to the elementary cell of the array, which is determined by the array period L. This converts the computational domain from infinite stripe into a rectangle, and enables the solving of the single-band Schrödinger equation in the new coordinates by straightforward implementation of the finite differences method.

The form of invertible coordinate transformation is given by:

$$\begin{aligned} x&=u;\\ y&=f(u,v). \end{aligned} \tag{3}$$

In order to describe the periodic array of QDHs and provide proper implementation of the boundary conditions, function $f(u, v)$ must be periodic with respect to u with period L. Moreover, suitable functions $f(u, v)$ should provide good fitting of the heterointerfaces in transversal plane, as well as rectangular profile of the well region within the elementary cell in the uv-space. Advantage of the approach based on coordinate mapping compared to direct implementation of FDM without the mapping is that potential problems with curvilinear boundary conditions or their careful implementation can be avoided.[14,15] Moreover, the profile of analyzed QDH can be varied simply by changing parameters of function $f(u, v)$.

By using coordinate transformations (3), Eq. (1) in the xy-space for $k_z = 0$ is mapped to equation:

$$-\frac{\hbar^2}{2}\left[\frac{\partial}{\partial u}\left(\frac{1}{m^*}\frac{\partial\psi}{\partial u}+\frac{\mu}{m^*}\frac{\partial\psi}{\partial v}\right)+\mu\frac{\partial}{\partial v}\left(\frac{1}{m^*}\frac{\partial\psi}{\partial u}+\frac{\mu}{m^*}\frac{\partial\psi}{\partial v}\right)+\rho\frac{\partial}{\partial v}\left(\frac{\rho}{m^*}\frac{\partial\psi}{\partial v}\right)\right]+U\psi=E\psi, \tag{4}$$

in the uv-space, where $\psi(u,v)=\psi[x(u,v),y(u,v)]$, $U(u,v)=U[x(u,v),y(u,v)]$, $m^*(u,v)=m^*[x(u,v),y(u,v)]$. According to the inverse function theorem, $\mu(u,v)$ and $\rho(u,v)$ are given by $\mu=\mu(u,v)=v_x=-f_u/f_v$, $\rho=\rho(u,v)=v_y=1/f_v$, where f_u and f_v denote partial derivatives of $f(u, v)$ with respect to u and v. Jacobian matrices J_{uv} and J_{xy} of transformation (3) and inverse transformation, respectively, are

$$J_{uv}=\begin{bmatrix}x_u & x_v\\ y_u & y_v\end{bmatrix}=\begin{bmatrix}1 & 0\\ f_u & f_v\end{bmatrix}, \tag{5a}$$

$$J_{xy}=\begin{bmatrix}u_x & u_y\\ v_x & v_y\end{bmatrix}=\begin{bmatrix}1 & 0\\ -f_u/f_v & 1/f_v\end{bmatrix}=\begin{bmatrix}1 & 0\\ \mu & \rho\end{bmatrix}, \tag{5b}$$

so that invertibility condition of transformation (3) is simply $|J_{uv}|=|J_{xy}|^{-1}=f_v\neq 0$. The form of transformation (3), as well as the periodicity of $f(u, v)$, provide that the periodic boundary condition (2) in the xy-space maps correctly into the uv-space and incorporates in the FDM scheme in straightforward manner. In case that $f(u, v)$ was an aperiodic function, the mapped space beyond the boundaries of the cell would be improperly mapped, which might lead to degradation of the boundary conditions.

The function $f(u, v)$, as well as $\mu(u,v)$ and $\rho(u,v)$, are given by analytical expressions. In addition, the well region corresponding to the elementary cell is a rectangle in the uv-space [Fig. 1(b)]. The computational domain in the uv-space is also a rectangle which is chosen to be large enough to comprise the well region of the elementary cell and corresponding wavefunctions [Fig. 1(b)]. Thus Eq. (4) can be directly discretized by using standard central differences.[12] Since the periodicity exists only in the u-direction, we apply Dirichlet boundary condition in the v-direction, i.e., $\psi(u,v)=0$ at the edge of the computational domain in the v-direction ($|v|=D_v$). The boundary condition in the u-direction is $\psi(L/2,v)=\exp(\imath KL)\psi(-L/2,v)$. The implementation of the finite differences scheme provides that the boundary conditions on heterointerfaces are naturally built in into the discretization and need not be enforced explicitly.

If the upper heterointerface of the QDH can be fitted by $y=f(u,v_g)=g(u)$, where v_g is corresponding v coordinate, all introduced parameters can be related to function $g(u)$ as follows: $t_W=g(\pm L/2)$, $H=g(0)$ and finally $(H-t_W)/2=g(\pm W/2)-t_W$, as shown in Fig. 1. Due to the symmetry of the profile of QDHs in the array, $f(u, v)$ and $g(u)$ are even functions with respect to u.

We first introduce transformation which provides fitting of the Gaussian-like QDH profile, given by following analytical expression (Gauss-mapping):

$$\begin{aligned}x&=u,\\ y&=f(u,v)\\ &=\sinh(Av)\left\{D+F\exp\left[-C\sin^2\left(\frac{\pi}{L}u\right)\exp(-Bv^2)\right]\right\}.\end{aligned} \tag{6}$$

As we already mentioned, the function $g(u)=f(u,v_g)$, fits the upper heterointerface of QDH in the xy-space for $v=v_g$, while the lower heterointerface of QDH, represented by the straight line $y=0$, corresponds to $v=0$. However, v_g is also a fitting parameter, which depends on the actual dimensions of the QDH elementary cell and positive constants A, B, C, D and F. Although all these parameters generally provide the fitting of the QDH cross-section profile and the adequate shape and dimensions of the computational domain, each of them differently affects the fitting of various geometrical parameters of the QDH elementary cell. For example, parameters A and B provide control of the computational domain dimensions in the xy-space. Once A and B are adopted, it is possible to investigate other parameters as C, D and F, which are relevant for precise fitting of the upper heterointerface within the elementary cell of QDH array. For example, D and F are used to fit the thickness of the wetting layer, since for common C and B-values the expression for the wetting layer thickness $t_W=g(\pm L/2)=\sinh(Av_g)\{D+F\exp[-C\exp(-Bv_g^2)]\}$, besides a scaling cofactor $\sinh(Av_g)$, is dominantly determined by D and F. In addition, D and F considerably affect the fit of the QDH height, since $g(0)=\sinh(Av_g)(D+F)$. Finally, C is used to fit the QDH width and its Gaussian-like profile. By using relation (6) it is possible to calculate C, D and F for a wide range of geometrical parameters t_W, H, W.

We find that coordinate transformation (6) cannot be used for fitting QDH arrays with densely packed QDHs. In this case, W/L ratio is relatively large, causing that C, D and F may not be positive. Moreover, the coordinate transformation becomes noninvertible. In order to analyze QDH arrays with large values of W/L, we use another coordinate transformation (Atanh-mapping) given by:

$$\begin{aligned}x&=u,\\ y&=f(u,v)=\frac{\sinh(Av)}{D+\operatorname{arctanh}[C\sin^2(\pi u/L)]/\cosh(Bv)}.\end{aligned} \tag{7}$$

Here, positive parameters v_g and B are used to control dimension of the computational domain in the xy-space. Once v_g and B are fixed, Eq. (7) can provide positive parameters A, C and D in terms of t_W, H, W.

Fig. 2(a) shows the profiles of QDHs, fitted by Atanh-mapping [Eq. (7)], for which the dash width W and the

period L are comparable. It can be seen that such QDH dimensions (i.e., $W = 7$ nm and $L = 8$ nm) correspond to almost vertical edges of the QDH elementary cells, which is common profile in the case of densely packed QDH arrays. The profile obtained from Atanh-mapping for relatively small ratios (e.g., $W = 7$ nm, $L = 20$ nm), can be equally well fitted by Gaussian profile defined by Eq. (6). For much smaller W/L ratios, the profile of QDH heterointerface can be better fitted by Gauss-mapping than by Atanh-mapping, since Eq. (6) provides very small values W/L. Figs. 2(b) and 2(c) show profiles of QDH array for various heights and all other parameters fixed, obtained for Atanh-mapping and Gauss-mapping, respectively. It can be seen that Eq. (6), which is used for larger L and smaller W/L ratio, provides broad range of Gaussian or lens-like QDH profiles with different heights [Fig. 2(c)], while Eq. (7), specialized for smaller L and larger W/L ratio, enables fitting of triangular-like profiles [Fig. 2(b)]. Figs. 2(d) and 2(e) depict the profile families derived from Eqs. (7) and (6), respectively, for which we vary the width W and keep all other parameters fixed. It can be seen that variation of W in the case of Gauss-mapping, besides lens-like profile, provides bell-like profile, for which the width can be very small. On the other hand, Atanh-mapping may produce much larger variety of profiles, which range from concave to convex shapes [Fig. 2(d)].

III. RESULTS AND DISCUSSION

The method described in Sec. II is generalization of the method we implemented on a single QDH.[12] Here, we extend the method to the one-dimensional array of QDHs, by using periodic functions for fitting the array heterointerface.

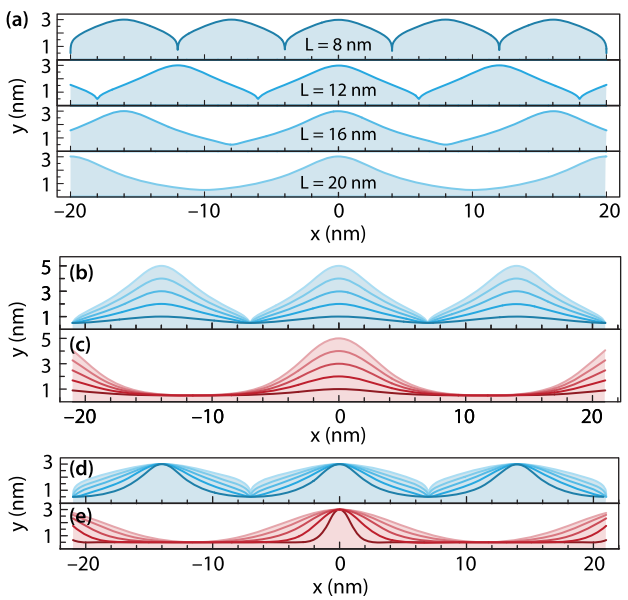

FIG. 2. Profile of the QDH cross-section (a) for $H = 3$ nm, $W = 7$ nm and various array periods $L = 8$, 12, 16, and 20 nm. Same for different heights $H = 1 - 5$ nm for QDH array with $W = 7$ nm and (b) $L = 14$ nm or (c) $L = 23$ nm. Same for different widths (d) $W = 4$, 6, 8, 10 and 12 nm for QDH array with $H = 3$ nm and $L = 14$ nm, and (e) $W = 2$, 4, 6, 8 and 10 nm for QDH array with $H = 3$ nm and $L = 23$ nm. Profiles in (a), (b), and (d) are obtained by fitting with Atanh-mapping, while (c) and (e) correspond to Gauss-mapping.

The efficiency and convergence of the method are already investigated and presented in the case of the single QDH.[12] Since the only significant change in the case of QDH array are fitting functions, which must satisfy the same conditions as those used for isolated QDHs, especially the invertibility condition described in the previous section, further investigation and characterization of the method are not needed. Essentially, the method proposed in Ref. 12 is revised to account for the periodic boundary conditions and instead of its implementation on an isolated QDH, it can be applied on the elementary cell of the QDH array. It means that method performances are not affected, as long as the invertibility condition is well satisfied.

In this section, we study the influence of geometrical parameters of the QDH array on its band structure. The analysis is based on the variation of the array period L, QDH width W and height H. In this study, the wetting layer thickness is set to $t_W = 0.5$ nm. However, the influence of the wetting layer thickness is also included in the discussion. In the analysis we vary one parameter at time, while other two are fixed and set to some average value. All calculations are performed for at least two different periods L, where one corresponds to large, while the others are for small W/L ratio. First, we study InAs/InAlGaAs QDH array, latticed matched to InP, and then QDH array based on InAs/GaAs which provides much deeper well.

Fig. 3 shows the miniband profile versus the array period L for two fitting functions, given by Eq. (7) [Figs. 3(a), 3(c), 3(f)] and Eq. (6) [Figs. 3(b), 3(d), 3(e), 3(g), 3(h)] for InAs/InAlGaAs QDH array. The QDH width is set to $W = 7$ nm, therefore for the range of period L from 8 to 20 nm it is more suitable to use Atanh-mapping since the ratio W/L is relatively large. For larger L, W/L ratio is smaller and much better fitting can be achieved by using Gauss-mapping. It can be seen that for densely packed QDHs there is a single and wide miniband [Fig. 3(a), $L < 12$ nm], which becomes narrower for increased period of the array and converges to the ground discrete state for $L > 25$ nm [Fig. 3(b)]. The coupling of QDHs also leads to formation of higher minibands, which become bound minibands for sufficiently large L ($L > 12$ nm). In other words, the excited minibands are part of the continuum for positive energies, i.e., small array periods. However, for large L, due to decreased quantum-mechanical coupling, these excited minibands become bound and narrower with respect to energy and tend to converge to the discrete excited states as the period increases. Finally, in the case of weak coupling between QDHs, i.e. for large L corresponding to almost isolated dashes, the band structure of the QDH array comprises one discrete state and wide band, consisting on a few almost joined minibands, close to the top of the well.

The variation of the QDH height H shows that for densely packed array, for which the ratio W/L is relatively large [Fig. 3(c)], height variation slightly affects the ground miniband width, especially for larger H-values. This result is not surprising, since the QDH coupling and consequently the miniband width depends on horizontal distance between the adjacent dashes (i.e., L or W) rather than on their vertical size. On the other hand, the variation of the QDH height H,

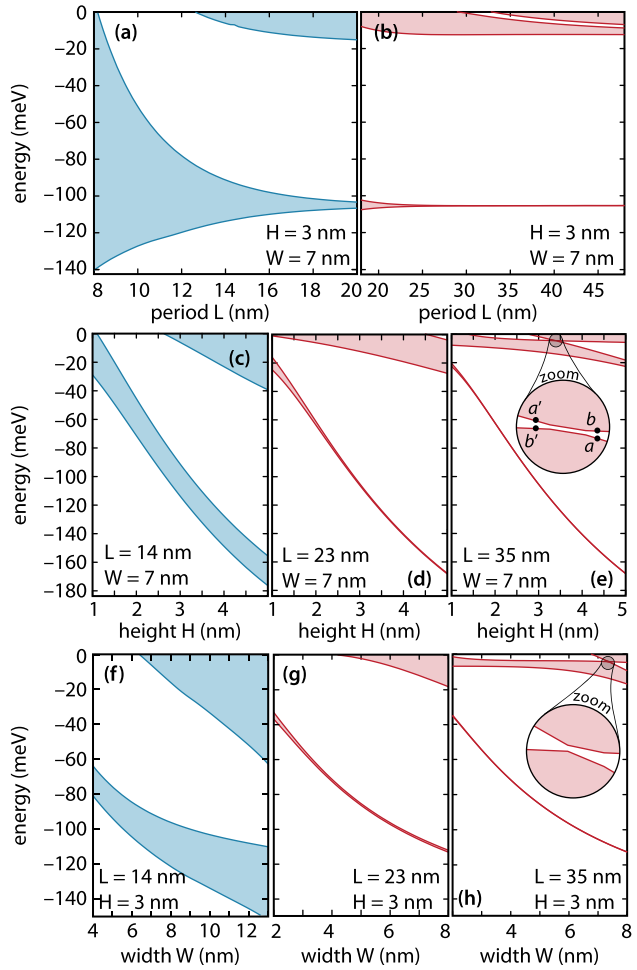

FIG. 3. The miniband structure for the periodic InAs/InGaAlAs QDH array with $t_W = 0.5$ nm with respect to (a)-(b) period L, (c)–(e) QDH height H, and (f)–(h) QDH width W. The miniband structure in (a), (c), and (f) correspond to QDH arrays obtained by fitting with Atanh-mapping, while those in (b), (d), (e), (g), and (h) correspond to the QDH arrays obtained by fitting with Gauss-mapping. Insets show zero-band-gap region between 2nd and 3rd miniband.

representing the QDH dimension in the direction of stronger confinement, leads to pronounced variation of the miniband energy. Similarly as for an electron in the infinitely deep quantum well, energy of which is inversely proportional to the square of the well width, the QDH miniband energy varies more rapidly with thickness variation for thinner than for thicker wells. Thus variation of the QDH height causes sudden change of the miniband energy. The dependence of the ground miniband width on H is, to some extent, different for relatively large L-values [Figs. 3(d) and 3(e)], since the miniband is already very narrow and its width slightly decreases with increase of H only for small H (1–2 nm). The reason is that increased H provides more space for the wavefunctions, which expand in the y- rather than in the x-direction, and in such way effectively reduces coupling among the dashes.

The increase of the dash width W, similarly as the increase of H, leads to the decrease of miniband energy. However, the width increase, for large W/L ratio, leads to the increase of the ground miniband width [Fig. 3(f)]. As a matter of fact, the width increase effectively decreases the period L, since the lateral sides of dashes come closer to each other [c.f. Fig. 2(a)]. As a result, the ground miniband becomes wider with increase of the QDH width. For smaller W/L ratio or large L, the QDH width weakly affects width of the minibands [Figs. 3(g) and 3(h)], although they decrease with W.

For sufficiently large L, the miniband dependence on width and height exhibits zero miniband gap effect (ZMBG), which can be observed for excited minibands, close to the top of the well [insets in Figs. 3(e) and 3(h)]. This effect is followed by miniband anticrossing. In other words, for the critical dimensions of QDH, the character of the top of the lower miniband is exchanged with the bottom of the higher miniband. The effect can be seen only for larger L, since the excited minibands, which are close to the well top, split due to the decrease of coupling, providing more minibands with smaller width. The effect can be also found in the case of variation of L, although it is not shown in figures.

The effect of zero miniband gap had been previously found in one-dimensional effective-mass superlattices.[16] It was shown that the effect can be noticed only for the minibands in the barrier (above the top of the well), in the case of variation of transversal, i.e., in-plane wave-vector k_t. The analytical treatment, which can be applied for the one-dimensional superlattices case, shows that the effect occurs for a certain conditions satisfied by the well and barrier width, and their corresponding effective masses. However, in the case of QDH array, the problem seems to be too complicated for analytical treatment. As it is shown in Fig. 3, the occurrence of the ZMBG effect depends on all three parameters (L, W, H). By using our numerical technique, we find that plots similar to Fig. 3 corresponding to $k_z > 0$ exhibit the shift of the ZMBG toward larger dimensions, i.e., larger L, W and H. The reason for this is the difference between the effective masses in the barrier and the well. Since the effective mass in the barrier is larger than the mass in the well, the increase of k_z effectively decreases the well depth, leading to weaker variation of subbands energy with dash dimension, than for $k_z = 0$. As a result, for $k_z > 0$, the ZMBG occurs for larger QDH dimensions, than for $k_z = 0$.

The presence of the wetting layer allows the barrier minibands to sink into the well and to exhibit the effect of zero miniband gap for energies for which the effect is not usually expected. Our calculation shows that the increase of the WL thickness increases the dash coupling and leads to the increase of the minibands width, their number and depth in the well. On the other hand, the decrease of the wetting layer to zero shows that the miniband structure almost completely disappears for large L, leaving only discrete energies. Consequently, the ZMBG effect is also vanishing in this case.

The ZMBG effect is followed by the anticrossing phenomenon, which is closely investigated in the case of height variation [zoom in Fig. 3(e)]. Fig. 4 shows the wavefunctions at the bottom of the 3rd and at the top of the 2nd miniband, for two height values, $H = 3.2$ nm and $H = 3.6$ nm, close to the critical height $H = 3.4$ nm, for which the zero miniband gap occurs. The boundary conditions at the extremes of the particular miniband (at its top and the bottom) have different sign of the phase shift factor $\exp(\imath KL)$, which can be $+1$ or

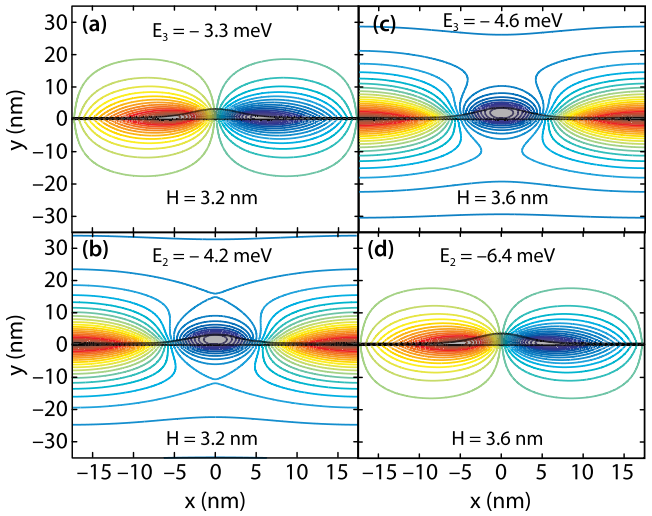

FIG. 4. Profile of the wavefunctions for QDH with $L = 35$ nm, $W = 7$ nm and $H = 3.2$ nm (a) at the bottom of the 3rd and (b) at the top of the 2nd miniband. (c) and (d): Same for $H = 3.6$ nm, respectively.

-1, depending on the miniband order. In addition, the sign of the phase factor, for the particular miniband extreme, according to the one-dimensional Kronig-Penney model, should alternate for adjacent minibands. According to this, the top of the 2nd and the bottom of the 3rd miniband should both correspond to the same, in this case, positive phase factor $(+1)$. In principle, the wavefunction of the higher miniband should have different parity or more precisely, larger number of nodes in one or the other confinement direction, than the lower miniband. Figs. 4(a) and 4(b) representing the wavefunctions of the states denoted by a' and b' in the inset of Fig. 3(e), show that the wavefunctions corresponding to height smaller than the critical ($H = 3.2$ nm) do not follow this rule. However, for heights larger than the critical [$H = 3.6$ nm, points b and a in the inset of Fig. 3(e)] the rule applies again [Figs. 4(c) and 4(d)]. This means that for the states at the top and the bottom of the adjacent minibands, for which the ZMBG occurs, swap the character, i.e., wavefunctions parity, while keeping the same phase factor.

In order to further investigate minibands in the QDH array, we calculate the band structure for deeper wells, which occur in InAs/GaAs QDH array. Fig. 5 shows the miniband profile versus dash period L, for larger W/L ratio [Fig. 5(a)] with fitting function given by Eq. (7), and for smaller W/L, corresponding to the fitting function (6) [Fig. 5(b)]. It can be seen that the number of minibands is increased, as one may expect, compared to the previous material system. In addition, the minibands more rapidly converge to discrete states with the increase in L. Similar results are obtained for variation of H [Fig. 5(c)–5(e)] and W [Fig. 5(f)–5(h)]. It should be noted that the effect of zero miniband gap is quite common in deeper wells. As shown in Figs. 5(e) and 5(h), it can occur more than once for particular miniband and cause alternation of the wavefunction parity for the considered range of geometrical parameters.

The material system of InAs/GaAs represents better environment for explanation of the ZMBG effect, than the previous one. In order to qualitatively explain the effect we closely inspect Fig. 5(h) and the anticrossing of the 2nd and

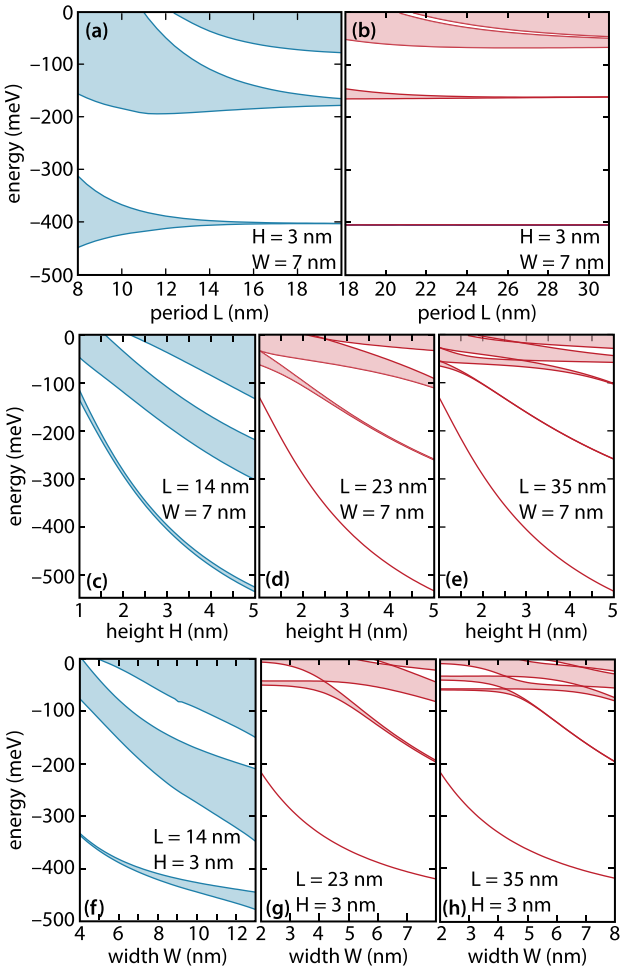

FIG. 5. The miniband structure for the periodic InAs/GaAs QDH array with $t_W = 0.5$ nm with respect to (a)–(b) period L, (c)–(e) QDH height H, and (f)–(h) QDH width W. The miniband structure in (a), (c), and (f) correspond to the QDH arrays obtained by fitting with Atanh-mapping, while those in (b), (d), (e), (g), and (h) correspond to the QDH arrays obtained by fitting with Gauss-mapping.

3rd miniband shown as schematics in Fig. 6. We start with small QDH widths ($W < 3$ nm), for which the wavefunctions of the 2nd and 3rd miniband are mainly situated in the wetting layer. This can be seen in the left column of Fig. 6 showing profiles of the wavefunctions for $W = 2.5$ nm. The widths of the minibands are very narrow. This is due to the fact that array period L is large enough that modulo of the wavefunctions corresponding to the extremes of the miniband are very similar, although the wavefunctions themselves have different parity due to the opposite phase factors. The increase of the QDH width provides more space for the wavefunction to accommodate into the QDH region. As long as the wavefunction is mainly situated into the wetting layer, the increase of the QDH width does not affect the miniband energy. Once the QDH width is large enough to accommodate a considerable part of the wavefunction, the increase of the QDH width will decrease the energy of the miniband or its extreme. However, due to different parity, the extremes of a miniband or the closest extremes of two adjacent minibands, have different critical widths for which their energy begins to decrease. For example, the top of the 2nd miniband has the same phase factor as the bottom of the 3rd miniband.

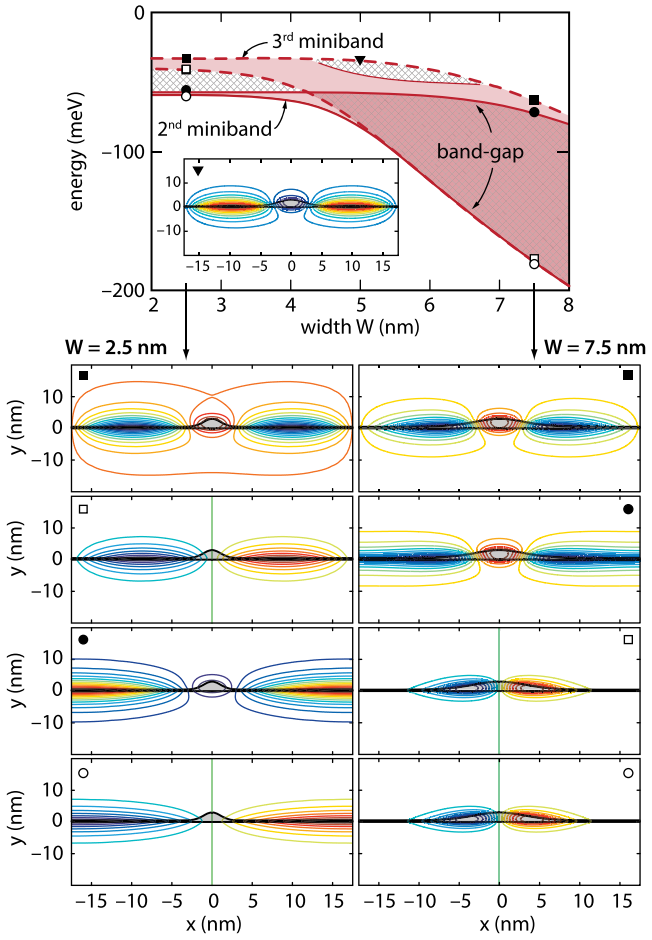

FIG. 6. Schematics of the ZMBG and anti-crossing effect between the 2nd and 3rd miniband for InAs/GaAs QDH array with $L = 35$ nm and $H = 3$ nm with respect to variation of QDH width W. Wavefunction profiles corresponding to $W = 2.5$, 5 and 7.5 nm are denoted with open and solid square, triangle, and dot markers.

In spite of that, the parity of these two wavefunctions is different, similarly as the parity of the top and the bottom of any of these two minibands. Due to larger number of nodes in the wavefunction (solid dot marker and corresponding wavefunction for $W = 2.5$ nm) the top of the 2nd miniband begins to decrease for larger widths than the bottom of the 3rd miniband, which wavefunction has smaller number of nodes (open square marker and corresponding wavefunction for $W = 2.5$ nm). Thus, for widths for which the bottom of the 3rd miniband decreases, the top of the 2nd miniband is almost constant. As a result, these two extremes approach each other, leading to the anticrossing of the minibands and the swap of the wavefunctions parity (solid dot and open square markers and corresponding wavefunctions profiles for $W = 7.5$ nm).

In general, the band structure at the top of the well consists of densely packed minibands, which represent a kind of so-called bound continuum. It can be expected that careful design of such complex continuum may provide efficient capture and relaxation of carriers into the QDH well, which might be essential for applications comprising optical transitions.

IV. CONCLUSIONS

The paper presents an efficient method for the calculation of the miniband structure of one-dimensional periodic QDH array, and based on the method, provides an analysis of its miniband character versus geometrical parameters. The method is a combination of the coordinate transformation of the QDH array and its vicinity into rectangular computational domain and the single-band Schrödinger equation solving in this domain by the finite differences method. The efficiency of the method is the result of array periodicity and carefully designed periodic fitting functions used for the coordinate transformation. The study of the minibands of the QDH array shows that miniband width is strongly related to the array period L and the wetting layer thickness t_W, although the width of QDHs may have significant impact for large ratio of the QDH width and array period. The miniband energy, on the other hand, considerably depends on the width W and the height H of QDHs in the array. For large periods L and some critical dimensions L, H or W, adjacent minibands in QDH array may exhibit the phenomenon of zero miniband gap, which is followed by the swap of the miniband character in its vicinity. Due to the wetting layer, higher minibands are clustered in the vicinity of the well top, providing a kind of the "bound continuum," which might be relevant for control of capture and relaxation of excited carriers.

ACKNOWLEDGMENTS

This work is supported by the Serbian Ministry of Science under project Photonics Components and Systems, No. 171011.

[1]E. A. Zibik, T. Grange, B. A. Carpenter, N. E. Porter, R. Ferreira, G. Bastard, D. Stehr, S. Winnerl, M. Helm, H. Y. Liu, M. S. Skolnick, and L. R. Wilson, Nature Mater. **8**, 803 (2009).
[2]V. Liverini, A. Bismuto, L. Nevou, M. Beck, and J. Faist, Appl. Phys. Lett. **97**, 221109 (2010).
[3]J. H. Wei and K. S. Chan, J. Appl. Phys. **97**, 123524 (2005).
[4]H. Dery, E. Benisty, A. Epstein, R. Alizon, V. Mikhelashvili, G. Eisenstein, R. Schwertberger, D. Gold, J. P. Reithmaier, and A. Forchel, J. Appl. Phys. **95**, 6103 (2004).
[5]M. Gioannini, IEEE J. Quantum Electron. **40**, 364 (2004).
[6]J. V. Crnjanski and D. M. Gvozdić, Acta Phys. Pol. A **116**, 668 (2009).
[7]J. V. Crnjanski and D. M. Gvozdić, Appl. Phys. Lett. **97**, 091906 (2010).
[8]J. V. Crnjanski, Phys. Scr. **T149**, 014034 (2012).
[9]M. Gioannini, IEEE J. Quantum Electron. **42**, 331 (2006).
[10]P. Miska, J. Even, C. Platz, B. Salem, T. Benyattou, C. Bru-Chevalier, G. Guillot, G. Bremond, Kh. Moumanis, F. H. Julien, O. Marty, C. Monat, and M. Gendry, J. Appl. Phys. **95**, 1074 (2004).
[11]A. Sauerwald, T. Kummell, G. Bacher, A. Somers, R. Schwertberger, J. P. Reithmaier, and A. Forchel, Appl. Phys. Lett. **86**, 253112 (2005).
[12]B. M. Stupovski, J. V. Crnjanski, and D. M. Gvozdić, Comput. Phys. Commun. **182**, 289 (2011).
[13]I. Vurgaftman, J. R. Meyer, and L. R. Ram-Mohan, J. Appl. Phys. **89**, 5815 (2001).
[14]T.-M. Hwang, W.-W. Lin, W.-C. Wang, and W. Wang, J. Comput. Phys. **196**, 208 (2004).
[15]T.-M. Hwang, W.-C. Wang, and W. Wang, J. Comput. Phys. **226**, 754 (2007).
[16]V. Milanović and Z. Ikonić, Phys. Rev. B **37**, 7125 (1988).